Weierstraß-Institut
für Angewandte Analysis und Stochastik

Leibniz-Institut im Forschungsverbund Berlin e. V.

Preprint ISSN 2198-5855

Self-consistent field theory for a polymer brush
Part I: Asymptotic analysis in the strong-stretching limit

Andreas Münch,[1] Barbara Wagner[2]

submitted: November 26, 2019

[1] Mathematical Institute
Andrew Wiles Building, Woodstock Road
Oxford, OX2 6GG
UK
E-Mail: muench@maths.ox.ac.uk

[2] Weierstrass Institute
Mohrenstr. 39
10117 Berlin
Germany
E-Mail: barbara.wagner@wias-berlin.de

No. 2648
Berlin 2019

2010 *Mathematics Subject Classification.* 74H10, 82B21.

2010 *Physics and Astronomy Classification Scheme.* 02.30.Mv, 61.25.H-.

Key words and phrases. Self-consistent field theory, asymptotic analysis, Cole-Hopf transformation, polymer brush.

Edited by
Weierstraß-Institut für Angewandte Analysis und Stochastik (WIAS)
Leibniz-Institut im Forschungsverbund Berlin e. V.
Mohrenstraße 39
10117 Berlin
Germany

Fax: +49 30 20372-303
E-Mail: preprint@wias-berlin.de
World Wide Web: http://www.wias-berlin.de/

Self-consistent field theory for a polymer brush
Part I: Asymptotic analysis in the strong-stretching limit

Andreas Münch, Barbara Wagner

Abstract

In this study we consider the self-consistent field theory for a dry, incompressible polymer brush, densely grafted on a substrate, describing the average segment density ϕ of a polymer in terms of an effective chemical potential μ for the interaction between the segments of the polymer chain. We present a systematic singular perturbation analysis of the self-consistent field theory in the strong-stretching limit, when the length scale of the ratio of the radius of gyration of the polymer chain to the extension of the brush from the substrate (ε) vanishes. Our analysis yields, for the first time, an approximation for the average segment density ϕ that is correct to leading order in the outer scaling and resolves the boundary layer singularity at the end of the polymer brush as $\varepsilon \to 0$. We also show that in this limit our analytical results agree increasingly well with our numerical solutions to the full model equations comprising the self-consistent field theory.

1 Introduction

The development of mean-field theories for polymeric systems that are able to make quantitative predictions for its wide-ranging applications requires these models to respect the architecture and type of monomers that make up the typically large macromolecules. The biggest challenge is how to coarse-grain the vast number of correlation with the surrounding macromolecules in order to faithfully predict the characteristic large-scale behaviour of the polymer system. In this respect self-consistent field theory (SCFT) has been extremely succesful since it was first introduced by Edwards [2] and Helfand [5] and since then has been extended to many polymeric systems ranging from block copolymer [6], polyelectrolytes [17] and many more, with applications ranging from cell biology, biomedical materials, to food science and innumerable soft-matter micro- and nanotechnological applications.

For the derivation of SCFT one uses the fact that the long polymer chains can be shown to obey a Gaussian distribution (Gaussian chain) and that monomers along the chain occur in repeat units that can be coarse grained into segments that still show a Gaussian distribution. This is also valid for Gaussian chains in an external field and eventually leads to expressions for the energy and hence the partition function in form of a functional integral (path integral) over all polymer configurations. This allows in principle the evaluation of the segment density distribution. Moreover, in the limit of small segments compared to the chain length, a leading order approximation for the partition functions, being functionals of the external field, can then be derived in terms of coupled Fokker-Planck type partial differential equations that have to be solved self-consistently.

However, even for the seemingly simple system of a polymer brush grafted on a substrate this can only be done numerically. A better understanding of grafted polymer brushes will be important for problems relating to surface functionalisation and designing surface properties that impact for example interface dynamics such as for example autophobic dewetting, or surface adhesion [3, 7, 8, 15].

DOI 10.20347/WIAS.PREPRINT.2648 Berlin 2019

In order to obtain analytical insights into the relation of the segment density distribution and the external field only further simplifications such as the so-called strong-stretching theory for dry polymer brushes in the limit of densely grafted polymer chains were so far successful.

The strong-stretching theory (SST) is valid when the chains are strongly stretched that is, their length L is much larger than the radius of gyration $R_g = a(N/6)^{1/2}$, which is the natural length scale for a polymer chain (a is the statistical segment length and N the number of segments in polymer chain). This can be expressed in the terminology of this paper as assuming that

$$\varepsilon \equiv \frac{aN^{1/2}}{\sqrt{6}\,L} \ll 1.$$

For SST the functional integral can be approximated using Laplace's method, when $\varepsilon \ll 1$, see [4]. For the derivation of the governing equations of self-consistent field theory the functional integrals are deformed in the complex plane before they are approximated by a saddle point approximation. This requires a much weaker assumption and in particular the SCFT is assumed to be valid for the range of $\varepsilon \ll 1$ on which the SST is based.

The question is therefore if the solutions obtained for the SST and the SCFT agree in the limit as $\varepsilon \to 0$, and for this purpose we will focus here on the problem of the tethered incompressible polymer brush. An important quantity is the energy of such a chain when it is stretched. The basic approximation of the SST for the effective chemical potential field μ is the parabolic potential, see [13]. For this the average segment concentration is a constant. It turns out that the SST leads to an asymptotic expansion in terms of ε for which the leading order and several corrections have been ingeniously obtained. Numerical comparisons with the energy of solutions to the SCFT are in agreement [12], validating the result. However, when we compare leading order approximations, this is not true. This is backed up by our numerical solutions and we find that it cannot be fixed by including only higher corrections in the potential μ. Obtaining the leading order (in ε) solution to the SCFT equations for ϕ for prescribed parabolic potential μ and showing that it differs from the constant is the main result of this paper. Our analysis reveals a surprisingly subtle asymptotic structure of the problem with several interlacing asymptotic layers in the segment length as well as the brush thickness.

In section 2 we give a formulation of the SCFT governing equations for a dry polymer brush consisting of identical polymer chains tethered to a wall or substrate. These consist of coupled Fokker-Planck type equations with an unknown field $\mu(x)$ and appropriate initial and boundary conditions. The Lagrange multiplier field is then determined from the expression for the segment density distribution $\phi(x)$ of the brush and the consistency requirement that the brush is incompressible. We then introduce an alternative formulation of the SCFT equations deriving Burger's type equations via a Cole-Hopf transformation.

Based on this formulation we derive the strong-sretching theory for "thick" brushes, where the dense grafting forces the chains to stretch to a brush thickness L that is large compared to the radius of gyration R_g. We give an argument why in the strong-streching limit the field $\mu(x)$ is approximated to leading order by a parabola.

This will then subsequently be used in section 3, where we present the complete asymptotic argument for solving for the partial partition functions. These results are used to construct the segment density distribution ϕ. Our analytical results are accompanied by numerical solutions. Our results demonstrate that $\phi(x)$ differs from the constant (in our (scaled) notation that constant is $\phi(x) = 1$) by $O(1)$. In fact the resulting $\phi(x)$ is singular at the boundary corresponding to where the brushes are tethered. We then determine the corrections to the parabolic $\mu(x)$, required in the asymptotic derivation to obtain

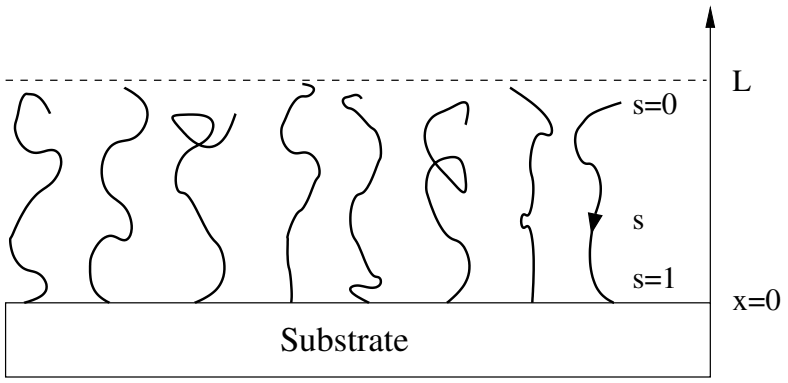

Figure 1: Schematic of a brush consisting of identical polymer chains, each consisting of N segments, grafted to a substrate at one end, with the other end being free. The brush extends to a thickness L, with $x = 0$ representing the surface of the substrate. The continuous variable $0 < s < 1$ labels sN-th segment of the polymer chain, starting from the free tip.

$\phi(x) = 1$ to leading order in ε. All our analytical results are compared to numerical simulations of SCFT in the limit $\varepsilon \to 0$.

2 Formulation

2.1 Basic model for a polymer brush

Here we formulate the model for an incompressible polymer brush, consisting of polymer chains that are densely grafted to a planar substrate at $x = 0$, using self-consistent field-theory. Following [1, 13], we assume that the chains consist of N segments which each have statistical length a. As an effect of the dense grafting, the polymer brush is extended to a length $x = L$. The model describes the average segment density $\phi(x)$ of the polymer segments in terms of an effective chemical potential $\mu(x)$ that describes the interaction between the chain segments, but it is not given explicitly. Rather, it is determined by the requirement that for an incompressible polymer brush, the density must be a constant. This is the "self-consistency" idea that underlies SCFT: The interactions are defined implicitly by a global constraint.

The density $\phi(x)$ is constructed for μ via two partition functions $q(x, s)$ and $q^*(x, s)$ that are used for obtaining the statistcs of the chain part with the free end at the edge of the brush and the other part that is grafted to the substrate, respectively. Specifically, the *partition function* $q(x, s)$ describes the density of end of a length sN, where $0 < s < 1$, if $s = 0$ end is free, and is given by the modified diffusion equation

$$\frac{\partial q}{\partial s} = \frac{a^2 N}{6}\frac{\partial^2 q}{\partial x^2} - \mu q, \tag{2.1a}$$

with initial and boundary conditions

$$q(x, 0) = 1, \tag{2.1b}$$

$$\frac{\partial q}{\partial x}(0, 0) = 0, \tag{2.1c}$$

$$\frac{\partial q}{\partial x}(L, 0) = 0. \tag{2.1d}$$

The position of a free end is arbitrary, hence $q(x,0)$ is constant, as in (2.1b). The situation at $x=0$ and $x=L$ is more delicate, as incompressibility breaks down close to the boundaries, i.e., $\phi(x)$ deviates from 1 close to $x=0,\,L$. This can be understood quite simply: The incompressibility condition would require ϕ to be 1 up to the boundary, but outside of the $[0,L]$, it is zero, but the density profile has to vary smoothly, contradicting incompressibility. This also implies that the potential μ is not defined within the SCFT theory but has to be found by other means, along with the true density, taking into account the details of the molecular interactions. The density profile and potential are then combined with the solution of (2.1) to give a distribution q on the entire domain $[0,L]$. In practice, however, the narrow regions at the boundaries are ignored, and the unmodified solution of (2.1) used instead; further details are given in [13].

Similarly, the *complementary partition function* $q^*(x,s)$ describes the density of end of a length sN, where the $s=0$ end is attached to the substrate, and is given by

$$\frac{\partial q^*}{\partial s} = \frac{a^2N}{6}\frac{\partial^2 q^*}{\partial x^2} - \mu q^*, \tag{2.2a}$$

$$q^*(x,0) = 2aN^{1/2}\delta(x), \tag{2.2b}$$

$$\frac{\partial q^*}{\partial x}(0,0) = 0, \tag{2.2c}$$

$$\frac{\partial q^*}{\partial x}(L,0) = 0. \tag{2.2d}$$

The only difference to (2.1) is in the initial condition, which requires the distribution q^* to collapse into a δ-function, as the position of the segment at $s=0$ is fixed at $x=0$.

The distribution of the segment s for the full chain is obtained by forming the product $q(x,s)q^*(x,1-s)$, noticing that the argument in q has been replaced by $1-s$ as it is assume that the $s=1$ end is the grafted end of the polymer, while $s=0$ is free. The distribution needs to be normalised, which is done with the help of the *full partition function*

$$Q = \frac{1}{L}\int_0^L q(x,s)q^*(x,1-s)\mathrm{d}x \tag{2.3}$$

It can be easily shown that Q is constant in s, and sometimes this can be used to simplify its evaluation by choosing a convenient s. Now we can obtain the average segment density as

$$\phi = \frac{1}{Q}\int_0^1 q(x,s)q^*(x,1-s)\mathrm{d}s, \tag{2.4}$$

The system is closed by the incompressibility condition

$$\phi(x) = 1.$$

Taken together, (2.1)-(2.4) constitute and inverse problem for μ.

Once the effective chemical potential is known, useful quantities can be computed. For polymer brushes, it is of interest to know their entropic free energy, which is given by

$$\frac{F}{nk_BT} = -\ln\left(\frac{QL}{aN^{1/2}}\right) - \frac{1}{L}\int_0^L \mu(x)\phi(x)\mathrm{d}x. \tag{2.5}$$

It is the difference of the total free energy, given by the first term on the right hand side, and the average internal energy for the interaction with the field μ, i.e. the second term.

Nondimensionalisation. To nondimensionalise these equations, we introduce

$$x = L\tilde{x}, \qquad \mu = \frac{\tilde{\mu}}{\varepsilon^2}, \tag{2.6}$$

where we have defined the dimensionless parameter ε as the ratio of the radius of gyration and the extension of the brush,

$$\varepsilon = \frac{R_g}{L} = \frac{aN^{1/2}}{\sqrt{6}\,L}, \tag{2.7}$$

The radius of gyration describes the natural size of the coiled up polymer chain, and is defined as the average density between the segments and the polymers center of mass. For ideal Gaussian chains, it is given by $R_g = a(N/6)^{1/2}$.

With these scalings, we obtain (after dropping the tildes) the following equations. For the partition function q, we have

$$\frac{\partial q}{\partial s} = \varepsilon^2 \frac{\partial^2 q}{\partial x^2} - \frac{\mu}{\varepsilon^2} q, \tag{2.8a}$$

$$q(x,0) = 1, \tag{2.8b}$$

$$\frac{\partial q}{\partial x}(0,0) = 0, \tag{2.8c}$$

$$\frac{\partial q}{\partial x}(1,0) = 0, \tag{2.8d}$$

and for the complementary partition function q^*,

$$\frac{\partial q^*}{\partial s} = \varepsilon^2 \frac{\partial^2 q^*}{\partial x^2} - \frac{\mu}{\varepsilon^2} q^*, \tag{2.8e}$$

$$q^*(x,0) = 2\sqrt{6}\,\varepsilon\delta(x), \tag{2.8f}$$

$$\frac{\partial q^*}{\partial x}(0,0) = 0, \tag{2.8g}$$

$$\frac{\partial q^*}{\partial x}(1,0) = 0. \tag{2.8h}$$

From this, we get

$$Q = \int_0^1 q(x,s) q^*(x,1-s) \mathrm{d}x \tag{2.8i}$$

$$\phi = \frac{1}{Q} \int_0^1 q(x,s) q^*(x,1-s) \mathrm{d}s. \tag{2.8j}$$

The incompressibility condition is unchanged,

$$\phi = 1. \tag{2.8k}$$

The entropic free energy of the brush is nondimensionalised

$$F = (nk_BT)\tilde{F}, \tag{2.9}$$

so we obtain (again dropping tildes),

$$F = -\ln\left(\frac{Q}{\varepsilon}\right) - \frac{1}{\varepsilon^2} \int_0^1 \mu(x)\phi(x) \mathrm{d}x. \tag{2.10}$$

2.2 Cole-Hopf transformation

In preparation for subsequent steps, we introduce the Cole-Hope transformation, which turns the modified diffusion equations into nonlinear, Burgers-type PDEs. In combination with the asymptotic analysis, this is equivalent to a WKB-type approach. We let $q = \exp(\sigma/\varepsilon^2)$, and $u = \partial_x \sigma$, giving

$$\partial_s u = \varepsilon^2 \partial_x^2 u + 2u\partial_x u - \mu_x, \tag{2.11a}$$

from (2.8a), and from (2.8b), (2.8c) and (2.8d) the initial and boundary conditions

$$u(x,0) = 0, \tag{2.11b}$$

$$u(0,s) = 0, \quad u(1,s) = 0. \tag{2.11c}$$

We can reconstruct q via $q = \exp(\sigma/\varepsilon^2)$, where

$$\sigma(x,s) = \int_a^x u(r,s)\mathrm{d}r + \int_0^s \varepsilon^2 \partial_x u(a,\omega) + u^2(a,\omega)\mathrm{d}\omega - \mu(a)s, \tag{2.12}$$

for any $0 \leq a \leq 1$. We will use in particular $a = 0$, for which we have

$$\sigma(x,s) = \int_0^x u(r,s)\mathrm{d}r + \int_0^s \varepsilon^2 \partial_x u(0,\omega)\mathrm{d}\omega - \mu(0)s. \tag{2.13}$$

So finding a solution for σ only requires the solution of a Burgers-type problem and a-posteriori integration of the Burgers solution u and its x-derivative with respect to x and s, respectively.

For the complementary variables, we analogously let $q^* = \exp(\sigma^*/\varepsilon^2)$, and $u^* = \partial_x \sigma^*$, and obtain from equivalent system to (2.8e), (2.8g) and (2.8h), which is

$$\partial_s u^* = \varepsilon^2 \partial_x^2 u^* + 2u^* \partial_x u^* - \mu_x, \tag{2.14a}$$

$$u^*(0,s) = 0, \quad u^*(1,s) = 0, \tag{2.14b}$$

$$\lim_{s\to 0^+} \partial_x u^*(x,s) = -\infty \qquad \text{for } x > 0. \tag{2.14c}$$

For the inverse transform, we can obtain σ^* via

$$\sigma^*(x,s) = \int_a^x u^*(r,s)\mathrm{d}r + \int_0^s \varepsilon^2 \partial_x u^*(a,\omega) + (u^*)^2(a,\omega)\mathrm{d}\omega - \mu(a)s + c_1(a), \tag{2.15}$$

and specifically for $a = 0$,

$$\sigma^*(x,s) = \int_0^x u^*(r,s)\mathrm{d}r + \int_0^s \varepsilon^2 \partial_x u^*(0,\omega)\mathrm{d}\omega - \mu(0)s + c_1(0). \tag{2.16a}$$

The constant $c_1(0)$ is determined by the requirement that the initial condition for σ^* has to satisfy the integral constraint implied by the appearance of the δ function in (2.8f), that is,

$$\lim_{s\to 0} \int_0^1 \exp\left(\epsilon^{-2}\sigma^*\right) \mathrm{d}x = \sqrt{6}\varepsilon.$$

Introducing (2.16) and using that

$$\int_0^x u^*(r,s)\mathrm{d}r = \frac{1}{2}\partial_x u^*(0,s)x^2 + O(x^3).$$

allows the integral to be evaluated in the usual manner for Laplace type integrals, provided that $\partial_x u(0,s) < 0$ giving

$$c_1(0) = \frac{1}{2}\ln\left(-\frac{12}{\pi}\lim_{s\to 0}\partial_x u^*(0,s)\right)\varepsilon^2. \tag{2.16b}$$

2.3 The parabolic approximation of the potential

For densely grafted polymer brushes, the chains are stretched well beyond their natural length, so that L is much larger than the gyration radius R_g, hence $\varepsilon \ll 1$. In this limit, an approximate strong stretching theory has been developed in place of the self-consistent theory presented above [13]. The leading order approximation for the potential is found to be, dimensionally,

$$\mu_{\text{dim},0} = -\frac{3\pi^2}{8a^2N} x_{\text{dim}}^2$$

and in our scalings (2.9)

$$\mu = -\frac{\pi^2}{16} x^2. \tag{2.17}$$

The strong-stretching theory has been refined by various authors [9–12, 14, 16] to obtain, for example, more accurate approximations of the entropic free energy. The expression given in [13] for example was obtained by a combination of calculating the contributions of various physical effects neglected in the basic strong-stretching theory and fitting. It becomes in our scalings

$$F = \frac{\pi^2}{48\varepsilon^2} - \ln\left(\frac{1}{2\sqrt{2}\,\varepsilon}\right) + 0.1544 - 1.2\varepsilon^{2/3} - 0.30\varepsilon^{4/3}. \tag{2.18}$$

In the following we will develop an asymptotic theory for the strong-stretching limit $\varepsilon \ll 1$ that directly recurs to the SCFT model (2.8) (and (2.10))) to compare with the results obtained by the authors above. We will do so in two steps. First, we will set μ equal to the parabolic approximation (2.17) and then use asymptotic expansions in ε to obtain approximations in particular for ϕ, as well as numerical solutions, and see that and by how much it violates the incompressibility condition (2.8k). Second, we will seek corrections to (2.17) via a similar route.

It turns out that the asymptotic structure in particular of u (and hence σ and q) is rather complicated; Fig. 2 gives and overview. There are three layers in s, $0 \le s \le 1$: A layer (labeled 1) close to the initial conditions, $s \ll 1$, an outer solution, labelled 2, where $s \sim 1$ and a layer labelled 3, where s is close to the end of the interval $s = 1 + \mathcal{O}(\varepsilon^2)$. The spatial structure in each of these regions is as follows:

- For s in region 1, the solution consists of an outer region 1A in x which where x preserves the scalings of (2.11a) and the asymptotic solution for u is linear in x, but does not satisfy the boundary condition, so that a boundary layer 1B is needed.
- As s increases, the latter splits into three regions, so that for s in region 2, there are five regions in x: The outer part 2A which is the continuation of $1A$; another outer region 2C and a corner layer 2B joining the two, and finally a boundary layer 2D to fix a higher order discontinuity at $x = 1$.
- As $s \to 1$, the left outer region and the corner layer are replaced by a boundary layer 3A, while the right outer region 3B and the boundary layer 3C at $x = 1$ preserve their structure.

We will discuss these regions and the asymptotic approximations there in section 3.1, starting with s in region 2 and the matching to region 1 and 3.

In contrast, u^*, and hence σ^* and q^*, only have two s-regions.

- An outer region in s, region 1, which consists of an outer region 1A in x which has the original scalings of (2.11a) but does not satisfy the boundary condition at $x = 1$, thus requiring a boundary layer 1A that is thinner than the boundary layer there for u.

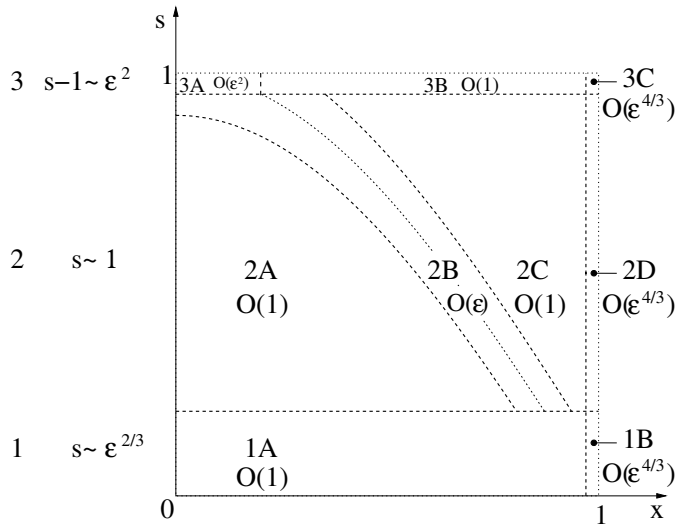

Figure 2: Map of the asymptotic regimes for u (and hence for q). There are three regimes in s, labelled 1-3 to the right of the vertical axes, where the corresponding scalings for s are also shown. For each s-regime, the x-regimes are counted by capital letters. The regimes are delineated by dashed lines. Each s and x regime is labelled by a combination of a number and a letter for s and x, respectively. The $O(\cdot)$ symbol indicates the scaling for x. Notice that for some of the layers, x is shifted as well as rescaled. The dotted line in the middle represents the centre of a corner layer that joins the two outer solutions in 2A and 2C. Details are given in subsequent sections.

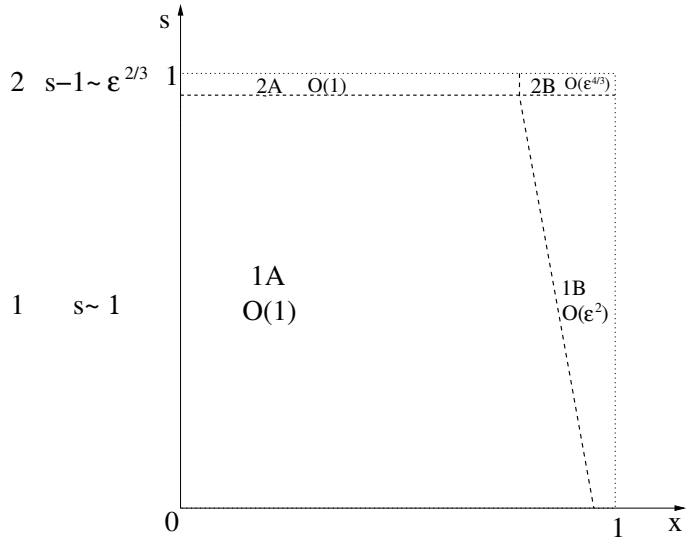

Figure 3: Map of the asymptotic regimes for u^* (and hence for q^*). Notation and conventions carry over from fig. 2. The regime 2B has an x-scaling that formally is $\mathcal{O}(\varepsilon^2)$, but the width of solution increases, so a tilted line was drawn to suggest this.

- As s approaches, the outer scaling of x is preserved in 2A but the boundary layer widens (in fact, like $\cot(\pi s/2)$ until the approximation is no longer valid and a new scaling has to be used. This defines the overall scaling of s in region 2, and the scaling of x in 2B.

In section 3.2, we give details and develop the asymptotic solutions, discussing the s-regions in their natural order.

3 Asymptotic analysis for a parabolic potential

3.1 Partition function

3.1.1 Outer region in s (region 2)

We first consider the situation where s and $1-s$ are $\mathcal{O}(1)$, which is the s-region 2 in Fig. 2.

Outer regions in x (regions 2A and 2C). We expand

$$u = u_0 + \varepsilon^2 u_1 + \dots. \tag{3.1}$$

To leading order, we obtain

$$\partial_s u_0 - 2u_0 \partial_x u_0 = \frac{\pi^2}{8} x. \tag{3.2}$$

For the initial and boundary conditions, we retain (2.11b) and (2.11c), respectively, to leading order. Characteristics satisfy the ODE system

$$\partial_t s = 1, \quad \partial_t x = -2u_0, \quad \partial_t u_0 = (\pi^2/8)x. \tag{3.3}$$

The characteristics enter the domain $0 < x < 1, 0 < s < 1$ either from the bottom, through $s = 0$, or from the right boundary, i.e. through $x = 1$. In the former, the initial curve is

$$s(0,\xi) = 0, \quad x(0,\xi) = \xi, \quad u_0(0,\xi) = 0, \qquad 0 < \xi < t, \tag{3.4}$$

giving the characteristics

$$s = t, \quad x = \xi \cos(\pi t/2), \quad u_0 = \frac{\pi}{4}\xi \sin(\pi t/2). \tag{3.5}$$

Notice that the characteristics all meet at $s = 1$, $x = 0$, and only cover the part of the domain for which $x \le \cos(\pi s/2)$. In terms of the original variables, we obtain for u_0

$$u_0 = \frac{\pi}{4} x \tan(\pi s/2) \quad \text{for} \quad x \le \cos(\pi s/2). \tag{3.6}$$

Notice that because of the constraint of x, the solution remains bounded even as s approaches 1.

For the characteristics entering from the right boundary, the initial condition is

$$s(0,\xi) = \xi, \quad x(0,\xi) = 1, \quad u_0(0,\xi) = 0, \tag{3.7}$$

giving

$$s = t + \xi, \quad x = \cos(\pi t/2), \quad u_0 = \frac{\pi}{4} \sin(\pi t/2), \tag{3.8}$$

hence $x = \cos(\pi(s-\xi)/2)$, and

$$u_0 = \frac{\pi}{4}\sqrt{1-x^2} \quad \text{for} \quad x > \cos(\pi s/2). \tag{3.9}$$

Corner layer (region 2B). The two parts of the outer solution have a corner along the characteristic $x = \cos(\pi s/2$, and hence require the introduction of a corner layer. We introduce new variables

$$u = \alpha(\varepsilon)v + \frac{\pi}{4}\sin(\pi s/2), \quad x = \beta(\varepsilon)z + \cos(\pi s/2). \tag{3.10}$$

Matching to the two parts of u_0, which are linear as $x \to \cos(\pi s/2)^{\pm}$, requires $\alpha = \beta$, and then the equation in the new variables becomes

$$\partial_s v = \frac{\varepsilon^2}{\alpha^2}\partial_z^2 v + 2v\partial_z v + \frac{\pi^2}{8}z. \tag{3.11}$$

For the second derivative of v to enter the dominant balance requires $\alpha = \varepsilon$, thus giving the full equation, that is remaining terms gives $\alpha = \beta = \varepsilon$, thus

$$\partial_s v_0 = \partial_z^2 v_0 + 2v_0\partial_z v_0 + \frac{\pi^2}{8}z, \tag{3.12a}$$

as is typical for these types of problems. Matching to the outer solution on the left and right gives the far-field conditions

$$v_0 \sim z\frac{\pi}{4}\tan(\pi s/2) \quad \text{as } z \to -\infty, \tag{3.12b}$$

$$v_0 \sim -z\frac{\pi}{4}\cot(\pi s/2) \quad \text{as } z \to +\infty. \tag{3.12c}$$

which come from matching to the two parts of the outer leading order solution. Initial values come from (2.11b),

$$v_0(z, 0) = 0, \qquad -\infty < z < +\infty. \tag{3.12d}$$

Boundary layer at $x = 1$ (region 2D). For the boundary layer at $x = 1$, we use

$$u = \alpha(\varepsilon)w, \quad x = 1 - \beta(\varepsilon)z. \tag{3.13}$$

At $x \to 1^-$, we have $u_0 \sim (\pi/4)\sqrt{2(1-x)}$, which in the new variables is $\alpha w_0 \sim (\pi/4)\sqrt{2\beta z}$. Balancing this requires $\beta = \alpha^2$, so that (2.11a) becomes

$$\alpha\partial_s w = \frac{\varepsilon^2}{\alpha^3}\partial_z^2 w - 2w\partial_z w + \frac{\pi^2}{8}(1 - \alpha^2 z). \tag{3.14}$$

The only possible balance is between the second derivative of w and the $\mathcal{O}(1)$ terms on the right hand side, resulting in $\alpha = \varepsilon^{2/3}$. Thus, the leading order problem is

$$\partial_z^2 w_0 - 2w_0\partial_z w_0 + \frac{\pi^2}{8} = 0, \tag{3.15a}$$

$$w_0(0) = 0, \tag{3.15b}$$

$$w_0 \sim \frac{\pi}{2\sqrt{2}}\sqrt{z} \quad \text{as } z \to +\infty. \tag{3.15c}$$

where the second and third equation come from the second boundary condition in (2.11c) and from matching with the outer problem, respectively.

Integrating (3.15a) once gives the ODE

$$\partial_z w_0 - w_0^2 + \frac{\pi^2}{8}z = \frac{\pi^2}{8}z_1. \tag{3.16}$$

The integration constant z_1 represents a shift of w_0, hence we first consider the case $z_1 = 0$. Then the general solution is

$$w_0(z) = -\frac{\pi^{2/3}\left(c_2\,\mathrm{Ai}'\left(\pi^{2/3}z/2\right) + \mathrm{Bi}'\left(\pi^{2/3}z/2\right)\right)}{2\left(c_2\,\mathrm{Ai}\left(\pi^{2/3}z/2\right) + \mathrm{Bi}\left(\pi^{2/3}z/2\right)\right)}, \tag{3.17}$$

where Ai and Bi denote the Airy functions. Indeed, if we vary c_2 over all real numbers including the limiting cases $c_2 = \pm\infty$, the value of $w_0(0)$ achieves each real number exactly once. It turns out that the only solution that has the right far-field behaviour as required by (3.15c) is in fact the one for $c_2 \to \infty$. Upon reinstating the shift z_1, this gives

$$w_0(z) = -\frac{\pi^{2/3}\mathrm{Ai}'\left(\pi^{2/3}(z+z_1)/2\right)}{2\mathrm{Ai}\left(\pi^{2/3}(z+z_1)/2\right)}. \tag{3.18a}$$

Since the zeros of Ai and Ai′ alternate, and none of the former is allowed to correspond to a value of z in the range $z > z_1$ to avoid singularities, there is only one value of z_1 for which w_1 also satisfies (3.15b), which expressed in terms of the largest zero $\zeta_1 = -1.018792972$ of Ai′ is

$$z_1 = \frac{2}{\pi^{2/3}}\zeta_1 = -0.9499104982. \tag{3.18b}$$

For future reference, we also record the first terms in the far-field expansion of w_0,

$$w_0(z) \sim \frac{\pi}{2\sqrt{2}}z^{1/2} + \frac{\pi^{1/3}\zeta_1}{2\sqrt{2}}z^{-1/2} + \frac{1}{4}z^{-1} + \mathcal{O}(z^{-3/2}) \qquad z \to \infty. \tag{3.19}$$

3.1.2 Region 1: $s = \mathcal{O}(\varepsilon^{2/3})$.

The solution structure above is not valid for s close to 0, since it requires the corner layer and the boundary layer to be well separated by the outer layer. The corner layer is the wider of the first two and has width $\mathcal{O}(\varepsilon)$, so validity requires that $s \gg \varepsilon^{1/2}$. To capture the behaviour near 0, we rescale $s = \delta\tilde{s}$, $u = \delta\tilde{u}$, with $\delta \ll 1$, and obtain from (2.11a)-(2.11c) the equation

$$\partial_{\tilde{s}}\tilde{u} = \delta\varepsilon^2\partial_x^2\tilde{u} + 2\delta^2\tilde{u}\partial_x\tilde{u} + \frac{\pi^2}{8}x \tag{3.20a}$$

and the initial and boundary conditions are

$$\tilde{u}(x,0) = 0, \tag{3.20b}$$

$$\tilde{u}(0,\tilde{s}) = 0, \quad \tilde{u}(1,\tilde{s}) = 0. \tag{3.20c}$$

We then expand $\tilde{u} = \tilde{u}_0 + \varepsilon^2\tilde{u}_1 + \cdots$, and obtain the leading order solution

$$\tilde{u}_0 = \frac{\pi^2}{8}x\tilde{s}. \tag{3.21}$$

This solution does not satisfy the boundary condition at $x = 1$. We therefore let $x = 1 - \alpha z$, giving

$$\partial_{\tilde{s}}\tilde{u} = \frac{\delta}{\alpha^2}\varepsilon^2\partial_z^2\tilde{u} + 2\frac{\delta^2}{\alpha}\tilde{u}\partial_z\tilde{u} + \frac{\pi^2}{8}(1-\alpha z) \tag{3.22}$$

We expect the second derivatives to enter in this layer, as they are most likely to provide a smooth transition. Hence we must have $\alpha = \varepsilon\delta^{1/2}$. For consistency, the first derivative term must not be

dominant. Sub-dominance requires $\delta^2/\alpha \ll 1$, and using the previous relation gives $\delta \ll \varepsilon^{2/3}$. The first derivative term enters the balance if $\delta = \varepsilon^{2/3}$. Using this gives

$$\partial_{\tilde{s}}\tilde{u} = \partial_z^2\tilde{u} + 2\tilde{u}\partial_z\tilde{u} + \frac{\pi^2}{8}(1-\varepsilon^{4/3}z). \tag{3.23}$$

Thus, to leading order

$$\partial_{\tilde{s}}\tilde{u} = \partial_z^2\tilde{u} + 2\tilde{u}\partial_z\tilde{u} + \frac{\pi^2}{8}, \tag{3.24a}$$

with boundary and far-field conditions

$$\tilde{u}(0,\tilde{s}) = 0, \tag{3.24b}$$

$$\tilde{u} \sim \frac{\pi^2}{8}\tilde{s} \quad \text{as } z \to -\infty. \tag{3.24c}$$

We need to join this with the $s = \mathcal{O}(1)$ region (s-region 2) that we analysed in the previous subsection. For this purpose, we need to understand the large $\hat{s}$ asymptotics of (3.24a). We rescale $\tilde{s} = \hat{s}/\delta_1$ with $\delta_1 \ll 1$. Introducing this into (3.24a) gives

$$\delta_1\partial_{\hat{s}}\tilde{u} = \partial_z^2\tilde{u} + 2\tilde{u}\partial_z\tilde{u} + \frac{\pi^2}{8}, \tag{3.25}$$

so that to leading order, we recover the problem (3.15).

This boundary solution has to be matched to a wider region to the left, so we scale $\hat{u} = \alpha\tilde{u}$, $\hat{z} = \beta z$ with $\beta \ll 1$ Since it satisfies the same problem (3.15), its far-field behaviour for $z \to \infty$ is the same as in (3.15c) and hence matching requires $\beta = \alpha^2$. Introducing this into (3.25) gives

$$\frac{\delta_1}{\alpha}\partial_{\hat{s}}\hat{u} = \alpha^3\partial_{\hat{z}}^2\hat{u} + 2\hat{u}\partial_{\hat{z}}\hat{u} + \frac{\pi^2}{8}\left(1 - \frac{\varepsilon^{4/3}}{\alpha^2}\hat{z}\right). \tag{3.26}$$

Since $\alpha \ll 1$, the second derivative drops out. The next two terms on the right hand side are already contained in (3.24), hence to get anything new, we need to include at least either the last term on the right hand side or the term on the left hand side. It seems plausible to include the former, to get additional spatial information, which means $\alpha = \varepsilon^{2/3}$. But then we are back to scaling the spatial variable as in 2D. This suggests that the s-region 1 with scaling $s = \mathcal{O}\varepsilon^{2/3}$ matches directly into the s-region 2, where $s = \mathcal{O}(1)$.

3.1.3 Region 3: $s - 1 = \mathcal{O}(\varepsilon^2)$

As $s \to 1$, the corner layer approaches the point $x = 0$. We therefore expect the asymptotic structure we have found for $s = \mathcal{O}(1)$ to break down when $\cos(\pi s/2) - 1 = \mathcal{O}(\varepsilon)$, that is, when $s - 1 = \mathcal{O}(\varepsilon)$.

On the other hand, if we for the moment allow s to go beyond $s = 1$ and let $s \to \infty$, we see that it tends to a stationary solution satisfying

$$\varepsilon^2\partial_x^2 u + 2u\partial_x u + \frac{\pi^2}{8}x = 0, \tag{3.27a}$$

$$u = 0 \qquad \text{at } x = 0,\ 1. \tag{3.27b}$$

This boundary value problem has a triple layer solution, with the leading order outer solution given by (3.9), the layer at $x = 1$ of width $\mathcal{O}(\varepsilon^{2/3})$ with the solution as in (3.18), and finally a layer at $x = 0$ of width $\mathcal{O}(\varepsilon^2)$ where the solution satisfies (letting $x = \varepsilon^2 y$)

$$\partial_y^2 u + 2u\partial_y u = 0, \tag{3.28a}$$

$$u = 0 \qquad \text{at } y = 0, \tag{3.28b}$$

$$u \to \frac{\pi}{4} \qquad \text{as } y \to \infty. \tag{3.28c}$$

This has the solution

$$u(y) = \frac{\pi}{4} \tanh\left(\frac{\pi y}{4}\right). \tag{3.29}$$

We investigate the solution near $s \to 1$ by letting $s - 1 = \delta\tau$ and $x = \alpha y$, with $\delta \ll 1$ and $\alpha \ll 1$. We anticipate that we have to match to a constant inner limit of u_0 in (3.9), so we do not rescale u. Introducing these scalings into (3.9) gives

$$\frac{1}{\delta}\partial_\tau u = \frac{\varepsilon^2}{\alpha^2}\partial_y^2 u + 2\frac{1}{\alpha}u\partial_y u + \frac{\pi^2}{8}\alpha y. \tag{3.30}$$

The last term in the differential equation is sub-dominant. The first term on the right hand side is sub-dominant, too, unless α has at most the same order as ε^2. But then nothing new is gained compare to the right outer problem, and we would [likely] end up with the solution structure of the $s = \mathcal{O}(1)$ problem. Hence we insist on retaining the second order derivative term and let $\alpha = \varepsilon^2$, giving to leading order

$$\frac{\varepsilon^2}{\delta}\partial_\tau u = \partial_y^2 u + 2u\partial_y u + \frac{\pi^2}{8}\varepsilon^4 y, \tag{3.31}$$

with boundary condition

$$u(0, 0) = 0. \tag{3.32}$$

From matching to (3.9), we obtain

$$u \to \frac{\pi}{4} \qquad \text{as } y \to \infty, \tag{3.33}$$

Therefore, dropping the $\partial_\tau u$ term, we obtain the stationary solution (3.29) to leading order.

3.1.4 Corrections in the outer regions 2A and 2C.

Keeping in mind that the goal is to obtain a result for ϕ that is correct to $\mathcal{O}(1)$, and that this implies dividing σ by ε^2 and before taking the exponential, we expect to need next order corrections at least in some cases. We first investigate the corrections to the left outer layer, that is, for $x < \cos(\pi s/2)$. Expanding to next order gives

$$\partial_s u_1 - \frac{\pi}{2}x\tan(\pi s/2)\partial_x u_1 = \frac{\pi}{2}\tan(\pi s/2)u_1, \qquad x \le \cos(\pi s/2), \tag{3.34a}$$

with initial and left boundary condition

$$u_1(x, 0) = 0, \qquad u_1(0, s) = 0. \tag{3.34b}$$

Notice that u_0 is an exact solution of the full PDE (2.11), no correction terms appear in (3.34a). Since the initial and boundary condition are also zero, we expect u_1 to vanish. Indeed, if we introduce characteristic variables, we recover the first two equations in (3.5) and

$$\partial_s u_1 = \frac{\pi}{2}\tan(\pi s/2)u_1. \tag{3.35}$$

Together with the initial condition this gives

$$u_1 = 0 \quad \text{for } x < \cos(\pi s/2). \tag{3.36}$$

For $x > \cos(\pi s/2)$, we expect to get a correction in the outer of $\mathcal{O}(\varepsilon^{-2})$, but in fact, to match with the second term in the expansion (3.19) of w_0 we first need a correction of $\mathcal{O}(\varepsilon^{4/3})$, that is, we let

$$u = u_0 + \varepsilon^{4/3}u_1 + \dots \qquad x > \cos(\pi s/2).$$

The leading order solutions in 2C and 2D are constant in time and hence we can expect u_1 to be time-independent as well and to satisfy the ODE

$$\frac{\pi}{2}\sqrt{1-x^2}\partial_x u_1 - \frac{\pi x u_1}{2\sqrt{1-x^2}} = 0, \qquad x > \cos(\pi s/2). \tag{3.37}$$

Integrating once gives

$$\frac{\pi}{2}\sqrt{1-x^2}\, u_1 = \frac{\pi}{2}c, \tag{3.38}$$

with an integration constant c. This gives

$$u_1 = \frac{c}{\sqrt{1-x^2}}. \tag{3.39}$$

Finally, we match with the second term in (3.19) to get

$$u_1 = \frac{\pi^{1/3}\zeta_1}{2\sqrt{1-x^2}}, \qquad x > \cos(\pi s/2). \tag{3.40}$$

We also record the composite solution u_c of u_1 and w_0 that is correct up to $\mathcal{O}(\varepsilon^{4/3})$:

$$u_c = u_0(x) - \frac{\pi}{2\sqrt{2}}\sqrt{1-x} + \varepsilon^{2/3}w_0\left((1-x)\varepsilon^{-4/3}\right), \qquad x > \cos(\pi s/2), \tag{3.41}$$

where u_0 and w_0 are given by (3.9) and (3.18), respectively.

3.1.5 Reconstruction of the partition function q

We now have all information on u we need to reverse the Cole-Hopf transform and obtain approximations for σ and then for q. Using (2.12) (with $\mu(0) = 0$ for the parabolic potential) gives for fixed $0 \le x < \cos(\pi s/2)$,

$$\begin{aligned}\sigma(x,s) &= \int_0^x u_0(r,s)\mathrm{d}r + \int_0^s \varepsilon^2\partial_x u(0,\omega)\mathrm{d}\omega + o(\varepsilon^2)\\ &= \frac{\pi}{8}x^2\tan(\pi s/2) - \frac{1}{2}\ln\cos(\pi s/2)\varepsilon^2 + o(\varepsilon^2).\end{aligned} \tag{3.42}$$

The error $o(\varepsilon^2)$ may appear too pessimistic, since know from our previous derivations that u_0 is the full outer expansion to at least $\mathcal{O}(\varepsilon^4)$ (and we can in fact speculate it is correct to all orders). However, we have not included the corner layer contribution which contributes an error that grows to $\mathcal{O}(\varepsilon^2)$ as we approach $\cos(\pi s/2)$, but is smaller than that as long as $\cos(\pi s/2) - x \gg \varepsilon$.

For $\cos(\pi s/2) < x < 1$ fixed, we obtain

$$\sigma(x,s) = \sigma(\cos(\pi s/2), s) + \int_{\cos(\pi s/2)}^{x} u_0(r,s)\mathrm{d}r + O(\varepsilon^2), \tag{3.43}$$

where the error term comes from the integrating across the corner layer, from dropping u_1. In fact, if we continue towards $x \to 1$, this does not change, as integrating across the boundary layer provides an $\mathcal{O}(\varepsilon^2)$ contribution as well. Evaluating the first term on the right hand side using (3.42) (noting the ε^2-term this introduces is absorbed into the overall error of the same order), we get

$$\sigma(x,s) = \frac{\pi^2}{16}s + \frac{\pi}{8}\left[x\sqrt{1-x^2} - \arccos x\right] + O(\varepsilon^2) \qquad \text{if } \cos(\pi s/2) \le x \le 1. \tag{3.44}$$

Using these results to obtain an approximation for q gives ($0 \le x \le 1$),

$$q(x,s) = \begin{cases} \dfrac{1}{\sqrt{\cos(\pi s/2)}} \exp\left(\dfrac{\pi}{8}\dfrac{x^2}{\varepsilon^2}\tan(\pi s/2)\right)\left(1+\mathcal{O}(\varepsilon^2)\right) & \text{if } x < \cos(\pi s/2), \\ \exp\left(\dfrac{\pi^2 s}{16\varepsilon^2} + \dfrac{\pi}{8\varepsilon^2}\left[x\sqrt{1-x^2} - \arccos x\right]\right) g_\varepsilon & \text{if } \cos(\pi s/2) \le x. \end{cases} \tag{3.45}$$

The term $g_\varepsilon = g_\varepsilon(x,s)$ collects all the error terms for $x \ge \cos(\pi s/2)$ and we cannot say more than that it is not worse than $O(1)$. This seems very little, but due to the exponential pre-factor with an $O(\varepsilon^{-2})$-term in the exponent, it is still a correction that moreover will turn out not to matter for the quantities we need.

3.1.6 Comparison with numerical results

Numerical solutions for u are shown in Fig. 4 for $\varepsilon = 0.1$ for moderate values of s, that is, values that are not close to 0 or 1. The solution structure corresponding to regions 2A-2C are clearly visible, with the two outer solutions a straight line on the left and a sector of an ellipse to the right corresponding to regions 2A and 2C, joined by a corner layer predicted for region 2B, with a maximum at $x = 0.67$ for example for $s = 0.5$ (red line). This corner moves to the left i.e. to smaller values of x as s increases. The leading order analytic approximations (3.6) for region 2A (dashed lines of corresponding colour) are on top of the numerical solution for x below $\cos(\pi s/2)$, i.e. to the left of the corner layer.

In contrast, there is a noticeable difference to the leading order outer solution (3.9) for region 2C, shown by a dotted line for all $0 < x < 1$. Notice that only the part with $x > \cos(\pi s/2)$, in other words, to the right of the corner layer, is relevant for each s. The difference is typically in the range of about 0.04 for moderate x and decreases by a factor of 2.5 as ε is doubled. This is consistent with an $\mathcal{O}(\varepsilon^{4/3})$ error predicted in section 3.1.4. Indeed, if we compare with the partial composite solution u_c in (3.41) which incorporates the $\mathcal{O}(\varepsilon^{4/3})$ correction, the fit is much better (dashed line with bullets). Varying ε, we found that the remaining difference at $x = 0.5$ for example decreases quadratically with ε, suggesting that the next order correction is $\mathcal{O}(\varepsilon^2)$.

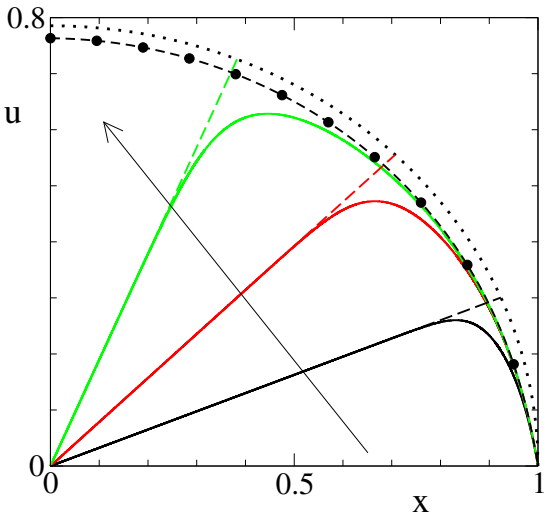

Figure 4: Comparison of the numerical solution of (2.11) (for the parabolic potential (2.17)), represented by solid lines, with the asymptotic approximations u_0 as in (3.60) and (3.9), shown by dashed and dotted lines, respectively. Notice that latter has been continued to $x = 0$. The partial composite solution (3.41) for $\varepsilon = 0.1$ is shown for $0 < x < 1$ by a dashed line emphasized by bullets. Numerical solutions for the same ε are shown for $s = 0.25, 0.5$ and 0.75 using black, red and green lines. The arrow points in the direction of increasing s.

3.2 Complementary partition function

3.2.1 Outer region in s (region 1)

For u^*, we first assume s and $1 - s$ are $\mathcal{O}(1)$. it turns out that we will only need two regions in s, one where $1 - s = \mathcal{O}(1)$ and a layer for $s \to 1$, but $s \ll 1$ does not require a special treatment as it was required for u. The full problem for u^* is given by (2.14) with μ set to parabolic chemical potential (2.17), that is

$$\partial_s u^* = \varepsilon^2 \partial_x^2 u^* + 2u^* \partial_x u^* + \frac{\pi^2}{8} x, \tag{3.46a}$$

$$u^*(0, s) = 0, \quad u^*(1, s) = 0. \tag{3.46b}$$

$$\lim_{s \to 0^+} u^*(x, s) = -\infty, \quad x > 0, \tag{3.46c}$$

Outer region in x (region 1A). We expand

$$u^* = u_0^* + \varepsilon^2 u_1^* + \dots, \tag{3.47}$$

giving, to leading order, the same PDE as for u_0,

$$\partial_s u_0^* = 2u_0^* \partial_x u_0^* + \frac{\pi^2}{8} x, \tag{3.48}$$

and the same boundary but different initial conditions, (3.46b) and (3.46c), respectively. The scale invariance of the problem without the boundary conditions is, however, the same, so we expect an expansion-type wave centred at $x = 0$ as before, however, in the case here it is concentrated at $x = 0$. Therefore, while the ODE system for the characteristics is again

$$\partial_t s = 1, \quad \partial_t x = -2u_0^*, \quad \partial_t u_0^* = (\pi^2/8)x. \tag{3.49a}$$

we parametrise the initial data via u_0 rather than parametrising x at $t = 0$,

$$s(0,\eta) = 0, \quad x(0,\eta) = 0, \quad u_0^*(0,\eta) = -\frac{\pi}{4}\eta, \tag{3.49b}$$

where the last expression needs to ensure that $u_0^*(0,\eta)$ spans the full range from 0 (to connect with the boundary condition $x = 0$) and $-\infty$, imposed by (3.46c). A linear function in η with the factor $\pi/4$ was chosen for convenience. The solution along characteristics is

$$s = t, \quad x = \eta \sin(\pi t/2), \quad u_0^* = -\frac{\pi}{4}\eta\cos(\pi t/2), \tag{3.50}$$

thus

$$u_0^* = -\frac{\pi}{4} x \cot(\pi s/2). \tag{3.51}$$

Boundary layer at $x = 1$ (region 1B). We need to introduce a boundary layer at $x = 1$. We need to match with

$$u_0^*(1,s) = -\frac{\pi}{4}\cot(\pi s/2), \tag{3.52}$$

which for moderate s is an $\mathcal{O}(1)$ constant, hence we only rescale x. Inner scaling of x increases the first and second derivatives in (3.46a), while keeping the other terms unchanged. So the natural balance is between the first two terms on the right hand side, giving

$$x = 1 - \varepsilon^2 z, \tag{3.53}$$

Introducing this and $U^*(z,s) = u^*(x,s)$ leads to the rescaled equation

$$\varepsilon^2 \partial_s U^* = \partial_z^2 U^* - 2U^* \partial_z U^* + \frac{\pi^2}{8}\varepsilon^2(1 - \varepsilon^2 z). \tag{3.54}$$

The leading order equation is

$$\partial_z^2 U^* - 2U^* \partial_z U^* = 0. \tag{3.55}$$

The solution that satisfies the boundary condition $U_0(0,s) = 0$ and matches to (3.52) is

$$U_0^* = -\frac{\pi}{4}\cot(\pi s/2)\tanh\left(\frac{\pi}{4}\cot(\pi s/2) z\right). \tag{3.56}$$

3.2.2 Region 2: $s-1=\mathcal{O}(\varepsilon^{2/3})$

Region 2B (inner region at $x=1$). The inner solution in region 1B will not last until $s=1$, since it decreases and widens until it has the same order as the other terms in (3.54). We can see from (3.56) that $U_0^* \sim \cot(\pi s/2)$ and $z \sim 1/\cot(\pi s)$, so that the two terms in the inner dominant balance scale like $\cot^3(\pi s/2)$. They balance with the two other terms, if $\cot(\pi s/2)=\varepsilon^{2/3}$. This suggests the following rescaling for region 2B:

$$z=\varepsilon^{-2/3}y, \qquad U^*=\varepsilon^{2/3}V^*, \qquad s=1+\varepsilon^{2/3}S. \tag{3.57}$$

Introducing this into (3.54) gives the equation

$$\partial_S V^* = \partial_y^2 V^* - 2V^*\partial_y V^* + \frac{\pi^2}{8}(1-\varepsilon^{4/3}y), \tag{3.58}$$

so to leading order

$$\partial_S V_0^* = \partial_y^2 V_0^* - 2V_0^*\partial_y V_0^* + \frac{\pi^2}{8}, \tag{3.59}$$

and boundary condition

$$V^*(0,s)=0. \tag{3.60}$$

We also need to match with (3.56). Taking the $s\to 1$ limit there, gives

$$U_0^* \sim \frac{\pi^2}{8}(s-1)\tanh\left(-\frac{\pi^2}{8}(s-1)z\right)+\mathcal{O}((1-s)^2). \tag{3.61}$$

Inserting (3.57) gives

$$V_0^* \sim -\frac{\pi^2}{8}S\tanh\left(\frac{\pi^2}{8}Sy\right) \quad \text{as } S\to-\infty. \tag{3.62}$$

Region 2A (outer region). To complete the discussion of region 2 and provide a matching condition for V^*, we now look at the outer spatial scaling for x, which in fact carries over from region 2A, since it still has width $\mathcal{O}(1)$. On the other hand, the magnitude of u^* needs to match with 2B so we take the scaling from the dependent variable from there. Combining the two, gives the following rescaling In terms of the new variables in 2B, we therefore have

$$x=1-\varepsilon^{4/3}y, \qquad \tilde{u}^*=V^*. \tag{3.63}$$

Using this in (3.58), we get

$$\partial_S \tilde{u}^* = \varepsilon^{8/3}\partial_x^2\tilde{u}^* + 2\varepsilon^{4/3}\tilde{u}^*\partial_x\tilde{u}^* + \frac{\pi^2}{8}x, \tag{3.64}$$

so to leading order

$$\partial_S \tilde{u}_0^* = \frac{\pi^2}{8}x, \tag{3.65}$$

which has the solution

$$\tilde{u}_0^* = \frac{\pi^2}{8}Sx, \tag{3.66}$$

where the integration constant has been fixed by matching back with (3.51). Notice this equation satisfies the boundary condition $\tilde{u}_0^*(0,S)=0$ at $x=0$. Rewriting (3.66) in terms of y and V^* gives the matching condition for V_0^*,

$$V_0^* \sim \frac{\pi^2}{8}S \quad \text{as } y\to\infty. \tag{3.67}$$

Notice that, because $S<0$, the limit of (3.62) as $y\to\infty$ agrees with (3.67).

3.2.3 Corrections in the outer region 1A

The next order correction to the outer problem is very similar to the problem for u_1,

$$\partial_s u_1^* + \frac{\pi}{2} x \cot(\pi s/2) \partial_x u_1^* = -\frac{\pi}{2} \cot(\pi s/2) u_1^*. \tag{3.68a}$$

with initial and left boundary condition

$$u_1^*(x,0) = 0, \quad u_1^*(0,s) = 0. \tag{3.68b}$$

Introducing characteristic variables, we get

$$\partial_s u_1^* = -\frac{\pi}{2} \cot(\pi s/2) u_1^*, \tag{3.69}$$

which has the general solution

$$u_1^* = \frac{A(\xi)}{\sin(\pi s/2)}. \tag{3.70}$$

However, the initial condition enforces $A(\xi) = 0$, hence

$$u_1^* = 0. \tag{3.71}$$

3.2.4 Reconstruction of the complementary partition function q^*

We can now obtain an approximation for q^* (via σ^*) from the information we have gathered on u^*. From (2.16), we get

$$\sigma^*(x,s) = \int_0^x u^*(r,s)\mathrm{d}r + \varepsilon^2 \int_0^s \partial_x u^*(0,\omega)\mathrm{d}\omega + \frac{1}{2} \ln\left(-\frac{12}{\pi} \partial_x u^*(0,0^+)\right) \varepsilon^2. \tag{3.72}$$

Introducing (3.51) gives, for fixed $0 \le x < 1$ and $0 < s < 1$,

$$\sigma^*(x,s) = -\frac{\pi}{8} x^2 \cot(\pi s/2) - \frac{1}{2} \ln \sin(\pi s/2) + \ln\left(\sqrt{3}\right) \varepsilon^2 + o(\varepsilon^2) \tag{3.73}$$

This solution needs to be changed or corrected in the initial and final s-layers and in the boundary layer near $x = 1$. The error estimate uses that u_1 is zero, so that there is no $\mathcal{O}(\varepsilon^2)$ contribution to the first term in (3.72), but in fact, we need a stronger assumption to ensure that the logarithmic term does not introduce and $\mathcal{O}(\varepsilon^2 \ln \varepsilon)$ term, namely that u_0 is correct to all orders at least at $x = 0$. From this we obtain

$$q^*(x,s) = \frac{\sqrt{3}}{\sqrt{\sin(\pi s/2)}} \exp\left(-\frac{\pi}{8\varepsilon^2} x^2 \cot(\pi s/2)\right) + o(1) \tag{3.74}$$

in the outer (s and x) region.

3.2.5 Comparison with numerical results

For the numerical solution, we regularise the δ-function in the initial condition for q^* by replacing it by a smooth approximation, that is, a suitable scaled Gaussian,

$$q^*(x,0) = \frac{2\sqrt{6}}{\sqrt{\pi}\omega\varepsilon} \exp\left(-\frac{x^2}{\omega^2 \varepsilon^4}\right). \tag{3.75}$$

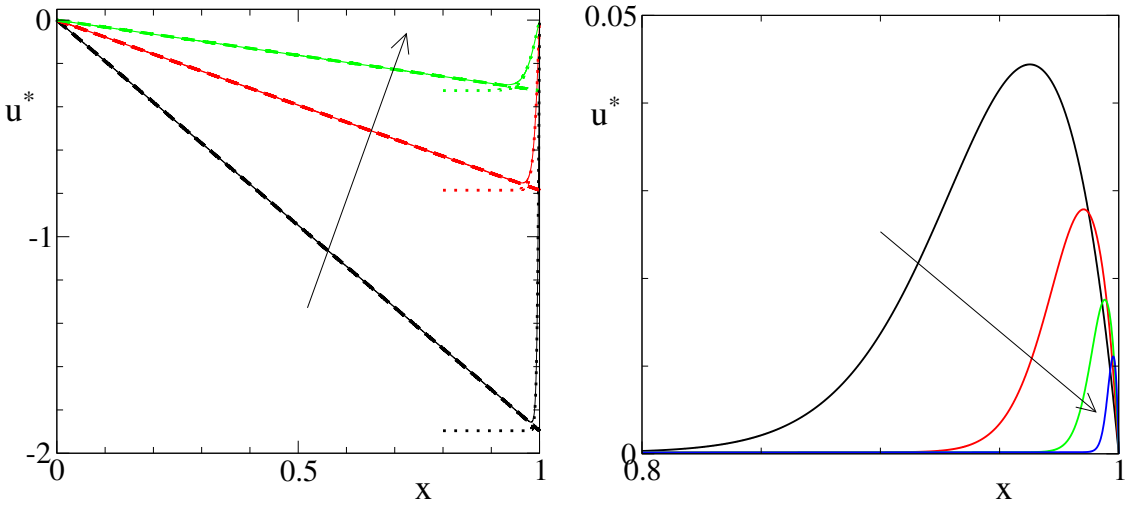

Figure 5: (a,left): Comparison of the numerical solution for u^* of (3.46) (and the regularised initial condition (3.77)), shown by solid lines, with the leading order asymptotic solution in region 1A (eqn. (3.77), dashed lines) and in region 1B (eqn. (3.56), dotted lines). The profiles are shown for $s = 0.25$, 0.5, and 0.75 using black, red and green lines, respectively. The arrow points in the direction of increasing s. (b, right): Numerical solution for u^* at $s = 1$ for $\varepsilon = 0.1$, 0.05, 0.025, 0.0125, and $\omega\varepsilon = 0.025$. The arrow points in the direction of decreasing ε.

The width of the Gaussian is chosen to be $O(\varepsilon^2)$ to ensure that it fits into the thinnest boundary layer near $x = 0$ anywhere in the problem, which is the one in section 3.1.3. From this, we obtain.

$$u^*(x,0) = -\frac{2x}{\omega^2\varepsilon^2}. \tag{3.76}$$

Unfortunately, this initial data does not satisfy the boundary condition $u = 0$ at $x = 1$. Hence we introduce a cut-off at $x = 1 - x_{\text{cut}}$, with $x_{\text{cut}} \ll 1$, and use the piecewise linear function

$$u^*(x,0) = \begin{cases} -\dfrac{2x}{\omega^2\varepsilon^2} & \text{if } 0 \le x \le x_{\text{cut}} \\ -\dfrac{2x_{\text{cut}}(1-x)}{\omega^2\varepsilon^2(1-x_{\text{cut}})} & \text{if } x_{\text{cut}} < x \le 1, \end{cases} \tag{3.77}$$

with $x_{\text{cut}} = 1 - \omega^2\varepsilon^4$. This choice is consistent with the boundary layer near $x = 1$ described by the scaling (3.53).

The numerical solutions in fig. 5(a) clearly shows the predicted structure. For small and moderate s not too close to 1, the outer approximation in region 1A (3.51) is a linear function in x that is on top of the numerical solution for $x < 1$. The outer approximation matches with the leading order boundary layer approximation (3.56), which in turn approximates the numerical solution very well in region 1B near $x = 1$. For $s \to 1$, the outer approximation remains valid but the boundary layer approximation does not. In particular for $s = 1$, both (3.51) and (3.56). While the numerical solutions shown in fig. 5(b) rapidly decay to zero away from $x = 1$, the are markedly non-zero near the end point. The figure shows the numerical results for several ϵ from 0.1 down to 0.0125. The value of the maximum decreases over this range by a factor of 4 and the position of the maximum by a factor of 16, which is consistent with the scaling predicted for region 2B (second equation in (3.57) and first equation in (3.63)).

3.3 Full partition function and density

3.3.1 Analytic approximations and error analysis

To calculate Q and ϕ, we need to obtain $q(x,s)q^*(x,1-s)$. We first note that for fixed $\cos(\pi s/2) < x < 1$, this expression becomes exponentially small, while for fixed $0 < x < \cos(\pi s/2)$, it is order one, so we can truncate the integrals to the latter region. Thus,

$$Q = \int_0^{\cos(\pi s/2)} q(x,s)q^*(x,1-s)\,\mathrm{d}x,$$
$$\phi(x) = \frac{1}{Q}\int_0^{(2/\pi)\arccos x} q(x,s)q^*(x,1-s)\,\mathrm{d}s.$$

Using (3.45) in the expression for Q gives

$$\begin{aligned} Q &= \int_0^{\cos(\pi s/2)} \frac{\sqrt{3}}{\cos(\pi s/2)}\,\mathrm{d}x + \mathcal{O}(\varepsilon) \\ &= \sqrt{3} + \mathcal{O}(\varepsilon). \end{aligned} \tag{3.78}$$

The error contribution from the outer layer is clear and is $\mathcal{O}(\varepsilon^2)$. However, we also integrate across boundary layers for which we have not included corrections. The largest boundary layer is the corner layer in u. Dropping the corner layer solution introduced an error $\mathcal{O}(\varepsilon)$ to u, but we need to integrate with respect to x to obtain σ, so we have an error of $\mathcal{O}(\varepsilon^2)$. Dividing by ε^2 and exponentiating to gives and $O(1)$ error to q and the product in the integrand of Q, but this only applies to the boundary layer so integration gives and $\mathcal{O}(\varepsilon)$ error as claimed.

Similarly,

$$\begin{aligned} \phi(x) &= \frac{1}{Q}\int_0^{(2/\pi)\arccos x} \frac{\sqrt{3}}{\cos(\pi s/2)}\mathrm{d}s + \mathcal{O}(\varepsilon), \\ &= \frac{2}{\pi}\ln\left(\frac{1+\sqrt{1-x^2}}{x}\right) + \mathcal{O}(\varepsilon). \end{aligned} \tag{3.79}$$

The error estimates follows from the same considerations as for Q and of course from the error present in Q itself.

3.3.2 Numerical comparisons

In this section, we are particularly interested in comparing the asymptotic and the numerical results for ϕ. As our base parameters, we choose

$$\varepsilon = 0.1, \quad \omega = 0.5. \tag{3.80}$$

In Fig. 6, we compare the analytic approximation for ϕ with the numerical results for the pair of values given in (3.80) and for the case where $\omega = 0.25$. The two numerical solutions and the analytical asymptotic approximation agree well except near the left and right end of the interval $0 < x < 1$. Changing ω hardly changes the numerical result near $x = 1$, but there is a noticeable difference near $x = 0$. However, this difference is not very large and in fact we found that the result converged to a

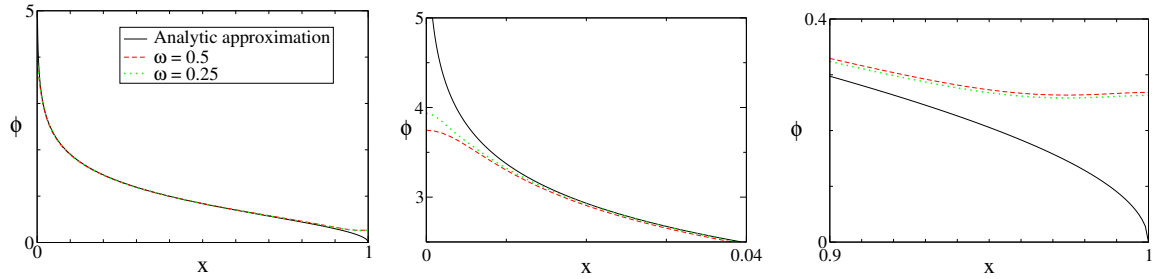

Figure 6: Comparison of analytical approximation for ϕ in (3.79) with two numerical solutions for two different ω, with $\varepsilon = 0.1$. Panel (a,left) shows the full view for $0 < x < 1$, while (b,middle) shows a zoom of the left end of the interval and (c,right) of the right end.

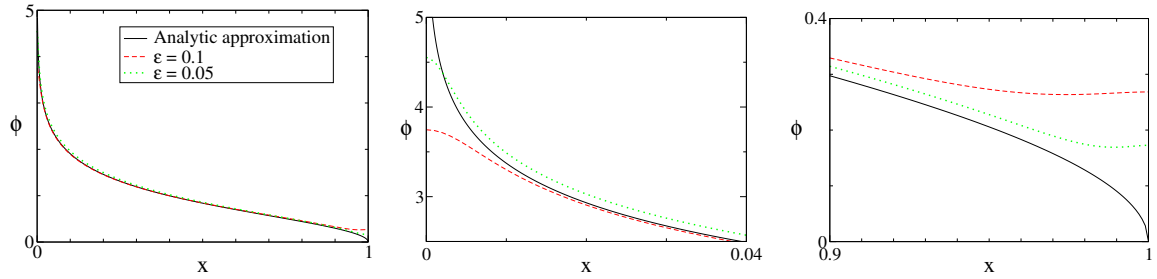

Figure 7: Comparison of analytical approximation for ϕ in (3.79) with two numerical solutions for two different ε, with $\omega\varepsilon = 0.05$ fixed. Panel (a,left) shows the full view for $0 < x < 1$, while (b,middle) shows a zoom of the left end of the interval and (c,right) of the right end.

finite curve as $\omega \to 0$, for fixed $\varepsilon > 0$. This is the limit in which the Gaussian approximation of the initial data for q^* becomes an exact δ-function. Thus we conjecture that for finite $\varepsilon > 0$, the solution for ϕ is finite and the logarithmic singularity in (3.79) is only recovered in the limit $\varepsilon \to 0$.

In Fig. 7, we keep $\omega\varepsilon$ fixed but decrease ε. Consistent with our previous remark, the value of the numerical solution for ϕ at $x = 0$ increases dramatically as ε is reduced, i.e. the graph of the numerical solution approaches the singularity of the analytical approximation (3.79) closer. At $x = 1$, the reduction of ε with fixed $\omega\varepsilon$ induces a change in the boundary layer, which becomes thinner. The zoom shows the situation, where the solution for the smaller ε has a deeper minimum that is closer to 1. The distance to 1 decreases from 0.026 to 0.011, that is, by a factor of 0.42; the prediction from the boundary layer analysis is $2^{-4/3} \approx 0.40$, so this is in reasonable agreement. The depth of the minimum changes from 0.26 to 0.17, or by 0.64, compared to $2^{-2/3} \approx 0.63$, again in reasonable agreement with the theoretical prediction from the boundary layer analysis.

4 Conclusion and Outlook

In this study we have used systematic singular perturbation analysis to establish analytically the strong-stretching limit of the self-consistent field theory for a dry polymer brush. The analysis lays the foundation to investigate the analytic expression for the polymer segment density as a function of the chemical potential (the external field) that is so far only known in the strong-stretching limit $\varepsilon \to 0$.

The asymptotic theory presented here is not restricted to the problem of a grafted brush but can be applied to other fundamental polymers systems such as homopolymer blends or diblock-copolymers

and will be addressed in our future work.

References

[1] A. Arora, J. Qin, D. C. Morse, K. T. Delaney, G. H. Fredrickson, F. S. Bates, and K. D. Dorfman. Broadly Accessible Self-Consistent Field Theory for Block Polymer Materials Discovery. *Macromolecules*, 49(13):4675–4690, July 2016. doi: 10.1021/acs.macromol.6b00107. URL http://dx.doi.org/10.1021/acs.macromol.6b00107.

[2] S. F. Edwards. The statistical mechanics of polymers with excluded volume. *Proceedings of the Physical Society*, 85(4):613–624, 1965. doi: 10.1088/0370-1328/85/4/301.

[3] R. Fetzer, K. Jacobs, A. Münch, B. Wagner, and T. P. Witelski. New slip regimes and the shape of dewetting thin liquid films. *Phys. Rev. Lett.*, 95:127801, 2005. doi: 10.1103/PhysRevLett.95.127801.

[4] G. Fredrickson. *The Equilibrium Theory of Inhomogeneous Polymers*. Oxford University Press, Dec. 2005. ISBN 978-0-19-856729-5. URL http://www.oxfordscholarship.com/view/10.1093/acprof:oso/9780198567295.001.0001/acprof-9780198567295.

[5] E. Helfand. Theory of inhomogeneous polymers: Fundamentals of the gaussian randomâĂŘwalk model. *The Journal of Chemical Physics*, 62(3):999–1005, 1975. doi: 10.1063/1.430517.

[6] E. Helfand and Z. R. Wasserman. Block copolymer theory. 4. narrow interphase approximation. *Macromolecules*, 9(6):879–888, 1976. doi: 10.1021/ma60054a001.

[7] G. Henn, D. G. Bucknall, M. Stamm, P. Vanhoorne, and R. JÃľrÃťme. Chain end effects and dewetting in thin polymer films. *Macromolecules*, 29(12):4305–4313, 1996. doi: 10.1021/ma9500392.

[8] H. Lee, W. Lee, Y. Soo Han, E. Kim, and D. Y. Ryu. Autophobic dewetting of polystyrenes on the substrates grafted with chemically identical polymers. *Polymer Journal*, 48:503 – 507, 2016. doi: https://doi.org/10.1038/pj.2016.10.

[9] A. E. Likhtman and A. N. Semenov. Theory of Microphase Separation in Block Copolymer/Homopolymer Mixtures. *Macromolecules*, 30(23):7273–7278, Nov. 1997. doi: 10.1021/ma9702713. URL http://dx.doi.org/10.1021/ma9702713.

[10] A. E. Likhtman and A. N. Semenov. An advance in the theory of strongly segregated polymers. *Europhysics Letters*, 51(3):307, 2000. URL http://stacks.iop.org/0295-5075/51/i=3/a=307. bibtex: 0295-5075-51-3-307.

[11] M. W. Matsen. Corrections to the strong-stretching theory of polymer brushes due to the entropy of the free ends. *The Journal of Chemical Physics*, 117(5):2351–2358, July 2002. doi: 10.1063/1.1487819. URL http://aip.scitation.org/doi/abs/10.1063/1.1487819.

[12] M. W. Matsen. Investigating the dominant corrections to the strong-stretching theory for dry polymeric brushes. *The Journal of Chemical Physics*, 121(4):1938–1948, July 2004. doi: 10.1063/1.1765101. URL http://aip.scitation.org/doi/10.1063/1.1765101.

[13] M. W. Matsen. Self-Consistent Field Theory and Its Applications. In G. Gompper and M. Schick, editors, *Soft Matter*, pages 87–178. Wiley-VCH Verlag GmbH & Co. KGaA, 2005. ISBN 978-3-527-61705-0. URL http://onlinelibrary.wiley.com/doi/10.1002/9783527617050.ch2/summary.

[14] M. W. Matsen. Strong-segregation limit of the self-consistent field theory for diblock copolymer melts. *The European Physical Journal E*, 33(4):297–306, Dec. 2010. doi: 10.1140/epje/i2010-10673-4. URL http://www.springerlink.com/index/10.1140/epje/i2010-10673-4.

[15] G. Reiter and R. Khanna. Negative excess interfacial entropy between free and end-grafted chemically identical polymers. *Phys. Rev. Lett.*, 85:5599–5602, Dec 2000. doi: 10.1103/PhysRevLett.85.5599.

[16] A. N. Semenov. Theory of block copolymer interfaces in the strong segregation limit. *Macromolecules*, 26(24):6617–6621, Nov. 1993. doi: 10.1021/ma00076a047. URL http://dx.doi.org/10.1021/ma00076a047.

[17] Q. Wang, T. Taniguchi, and G. H. Fredrickson. Self-consistent field theory of polyelectrolyte systems. *The Journal of Physical Chemistry B*, 109(19):9855–9856, 2005. doi: 10.1021/jp051804+.